Available online at www.sciencedirect.com
SCIENCE DIRECT
Journal of Power Sources 157 (2006) 166–176
JOURNAL OF POWER SOURCES
www.elsevier.com/locate/jpowsour

Behavior of PEMFC in starvation

Zhixiang Liu [a], Lizhai Yang [a], Zongqiang Mao [a,*], Weilin Zhuge [b], Yangjun Zhang [b], Lisheng Wang [c]

[a] *Institute of Nuclear and New Energy Technology, Tsinghua University, Beijing 100084, PR China*
[b] *Department of Automotive Engineering and The State Key Laboratory of Automotive Safety and Energy, Tsinghua University, Beijing 100084, PR China*
[c] *Beijing LN Power Sources Co. Ltd., Beijing 100094, PR China*

Received 1 July 2005; received in revised form 9 August 2005; accepted 10 August 2005
Available online 17 October 2005

Abstract

Starvation is a vivid word to describe the operation condition of a fuel cell in sub-stoichiometric reactants feeding. In starvation, a fuel cell could not present its best performance; moreover, there might also be safety issue because of cell reversal. In this paper, current density distributions of proton exchange membrane fuel cell (PEMFC) in hydrogen and air starvation were studied with a segmented single fuel cell. Experimental results show that the polarization curves of the overall cell are different for anode and cathode starvation. And the current density distribution results show that for anode starvation, current density of the starved region drops sharply to zero, while for cathode starvation, there is no zero current density region observed. Numerical simulations give similar results.

Keywords: Proton exchange membrane; Fuel cell; Starving operation; Current distribution

1. Introduction

Starvation, a quite vivid word to describe the operation condition of fuel cells in sub-stoichiometric fuel or oxidant feeding, is one of the potential causes for fuel cell failure. Many factors will lead to starvation in a fuel cell: poor cell design or machining with uneven mass distribution in flow fields, poor stack design or assembly with uneven flux distribution between cells, poor water management with channel block by flooding; poor heat management in cold startup with ice blocking, and misoperation with sub-stoichiometric gas feeding.

In a fuel cell stack, if some of the cells are in starvation, potential of these cells will drop to a lower level than others, which could be detected with cell voltage monitoring. If the starvation is not too serious and the reactants are enough to maintain the stack current, voltage of these cells will be positive though lower than others. However, if the fluxes of reactants are not enough to maintain the stack current, to balance the current value, there must be a part of electrolysis current which will make the voltage of the starved cells drop to negative—named "cell reversal". In the case of fuel starvation, because hydrogen is no longer enough to be oxidized to maintain the current, anode potential will increase high enough to make water oxidized in anode with oxygen produced. At the same time, oxygen is reduced in cathode, so the net effect is analogous to a bilateral selective "pump"—oxygen is pumped from cathode to anode while water from anode to cathode simultaneously. Oxygen production in anode has been proved with GC [1]. The electrode half reactions and the overall reaction are listed below:

$$\text{Anode}: \quad 2H_2O(a) \rightarrow O_2(a) + 4H^+ + 4e^-$$

$$\text{Cathode}: \quad O_2(c) + 4H^+ + 4e^- \rightarrow 2H_2O(c)$$

$$\text{Overall}: \quad O_2(c) + 2H_2O(a) \rightarrow 2H_2O(c) + O_2(a)$$

If the anode potential gets too high, for Pt/C anode catalyst, carbon is prone to be oxidized with the presence of platinum

* Corresponding author. Tel.: +86 10 62784827; fax: +86 10 62771150.
E-mail address: maozq@tsinghua.edu.cn (Z. Mao).

0378-7753/$ – see front matter © 2005 Elsevier B.V. All rights reserved.
doi:10.1016/j.jpowsour.2005.08.006

as catalyst:

$$C + 2H_2O \rightarrow CO_2 + 4H^+ + 4e^-$$

For the case of oxidant starvation, proton transport from anode will be oxidized in cathode to form hydrogen and the cell essentially acts as a hydrogen pump [1]:

$$\text{Anode :} \quad H_2(a) \rightarrow 2H^+ + 2e^-$$

$$\text{Cathode :} \quad 2H^+ + 2e^- \rightarrow H_2(c)$$

$$\text{Overall :} \quad H_2(a) \rightarrow H_2(c)$$

It could be seen that for both anode and cathode starvation, hydrogen and oxygen will mix inside the fuel cell. With the presence of catalyst, burning reaction is not evitable. There is even threat for explosion. So for a practical fuel cell stack, it should be carefully operated without starvation.

Starvation behavior of phosphoric acid fuel cell (PAFC) has been studied and reported by Mitsudo and Murahashi [2,3], Lundblad and Bjornbom [4] and Song et al. [5], but PEMFC starvation behavior is not well documented [6,7]. Taniguchi et al. [7] analyzed the electrocatalyst degradation during fuel starvation and found the anode ruthenium dissolution and cathode platinum sintering. Kim et al. [8] reported vacuum effect in anode starvation operation, which could cause fuel being drawn from the manifold in a stack or ambient air entering a laboratory scale cell. However, these papers did not indicate the current distribution information inside the fuel cell. In references [2,3], the authors used a single PAFC with a series of reference electrodes placed around the cell to study hydrogen and air starvation behavior. For proton exchange membrane fuel cell (PEMFC) and direct methanol fuel cell (DMFC), several groups have reported current density distribution measurement results [10–17]. In Yoon's paper [17], current distribution of the experimental cell under different degree of flooding was discussed; Hakenjos et al.'s [16] experimental system combined the current distribution, temperature distribution and flooding viewing into one cell; in Mench's DMFC system [14], different air stoichiometry is given to study the dynamic behavior of gradual flooding. These authors did not utilize their current density distribution measurement systems to examine the behavior of PEMFC in starvation operation. In this paper, we utilized our current distribution measurement system, which was reported in [10], to study the starvation behavior of a PEMFC single cell in detail. It should be confessed that it is more meaningful to study starvation in a fuel cell stack; however, such study is not easy because of the difficulty in current density distribution measurement in a stack.

2. Experimental

The current distribution measurement fuel cell system and the structure of the segmented anode plate are shown in Fig. 1. Twelve collectors were embedded in an end plate to collect the current of the segmented subcells. A detailed description could be found in our previous paper [10]. Active area of the membrane electrode assembly (MEA) is 30 cm^2, with Nafion® 112 membrane as the electrolyte.

Current of the each subcells were measured with a series of 10 mΩ current-viewing resistors, voltage shares of which were collected with computer and current could be calculated. The experiments were conducted with Arbin Fuel Cell Test Stand. Temperature of the fuel cell was controlled with warm water flew through the cooling plate (here actually acted as warming plate) on the cathode side. Hydrogen and air were humidified with membrane humidifier from Beijing LN Power Source Co. Ltd. In this experiment, temperature of the fuel cell and the humidifier were kept constant to be 70 °C.

3. Results and discussions

3.1. Cell performance in regular condition

For comparison, cell performance in regular condition was measured. Polarization curves of the overall cell and the subcells were recorded with sufficient hydrogen and air feeding. The voltage of the cell was controlled to decrease from the open circuit voltage to 0.25 V linearly with a scan rate 1 mV s^{-1}. Backpressures of the anode and cathode were kept to be 0.2 MPa (absolute pressure). The fluxes of H_2 and air were kept constant during the measurement. Flux of H_2: 0.32 SL min^{-1}, flux of air: 0.78 SL min^{-1}, which were 0.5 times in excess for the fuel cell to operate at 1 A cm^{-2} current density. The polarization curves of the overall cell and the subcells in the middle column (subcells 2, 5, 8 and 11) were shown in Fig. 2. From the figure, we can see that the curve of the overall cell is about the average of the subcells. The current density differences between the subcells are not too great when the cell voltage is higher than 0.7 V. However, the limiting current density is quite different: subcell 11 is less than 0.7 A cm^{-2}, while subcell 2 higher than 1.0 A cm^{-2}. There are at least two factors which will impact the current density difference along the flow channels: reactant concentration dropping and the saturation increasing. According to Fick's Law, diffusivity of oxygen through cathode GDL could be expressed in Eq. (1):

$$N_{O_2} = D\frac{c^0_{O_2} - c^*_{O_2}}{\delta} = \frac{I}{nF} \tag{1}$$

where $c^0_{O_2}$ and $c^*_{O_2}$ are concentration of oxygen in the flow channel and that on the catalyst surface, respectively, δ the thickness of GDL and D is diffusion coefficient. When the concentration of oxygen on the catalyst surface decreases to zero, the corresponding current is the limiting current, as shown in Eq. (2):

$$I_L = nFD\frac{c^0_{O_2}}{\delta} \tag{2}$$

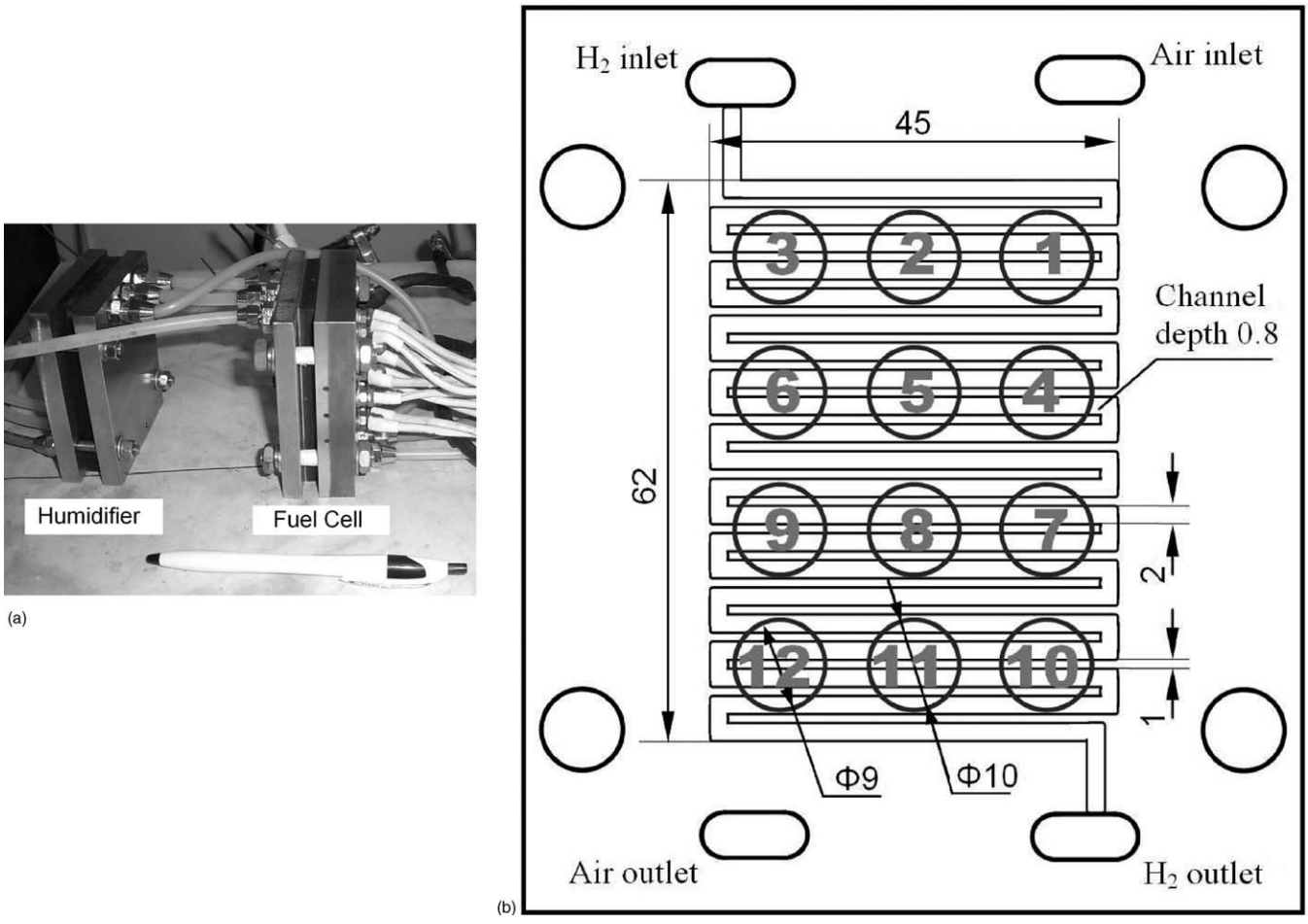

Fig. 1. Current density measurement system: (a) photograph of the experimental system and (b) structural plot of the anode plate (unit: mm).

where I_L is the limiting current. The equation shows proportional relationship between the limiting current and oxygen concentration in the flow channel, which could also be found with the experimental results given in reference [18]. On the other hand, as the humidifier is at the temperature to the fuel cell, electrode flooding (or at least partial flooding) is inevitable with a low stoichiometric ratio at high current density. Although the feed gas out of the membrane humidifier is not full saturated (experimental data show that relative humidity is higher than 90% [19]), it will be saturated very soon in the fuel cell under large load. The flooding of the electrode will become heavier and heavier along the flow channel, which will make the current density getting lower and lower. In Fig. 2, the current fluctuation of subcells 8 and 11 in low voltage region illustrates the influence of flooding.

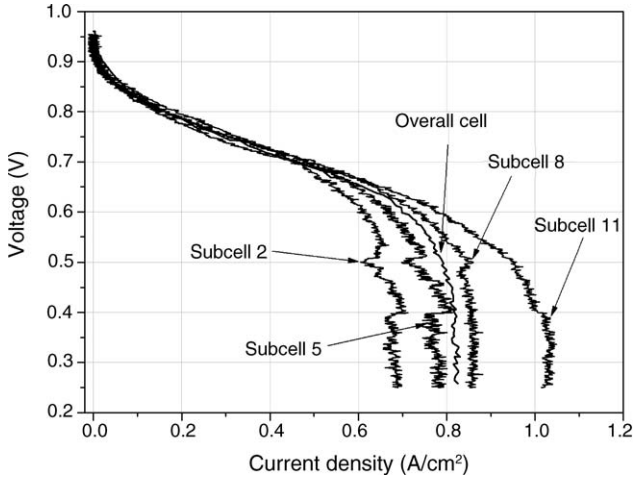

Fig. 2. Polarization curve of the overall cell and the subcells in the middle column. Cell temperature: 70 °C; humidifying temperature: 70 °C; pressure: 0.2 MPa; flux of H_2: 0.32 SL min^{-1}; flux of air: 0.78 SL min^{-1}; scan rate: 1 mV s^{-1}.

Fig. 3 shows the current density distribution of the fuel cell at different cell potential. The numbers of the subcells are also shown in the plot. It shows that when cell potential is relative high, at 0.8 V in this plot, current density of the outlet region is higher than that of the inlet region, while at lower cell voltage, 0.6 V and 0.5 V, current density of the outlet region is much lower than that of the inlet region. At 0.8 V, the average current density is about 150 mA cm^{-2}, and the stoichiometric ratio is about 10. Even though the feed gas is 100% saturated, the outlet gas is about 10% oversaturated. Liquid water might form in the pores of the GDL, however, with the hydrophobic character of the diffusion layer, flooding is not likely to occur. Along the channel, membrane

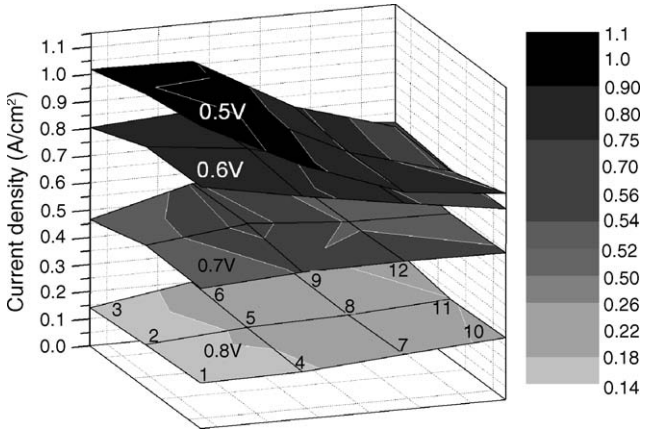

Fig. 3. Current density distribution at different cell potential.

near the outlet is better hydrated and has lower impedance, so better cell performance is shown. While at 0.6 V and 0.5 V, current density of the inlet region is much higher than the outlet region. A lower cell voltage will leads to higher current and lower stoichiometry and will increase oxygen concentration gradient along flow channel. Moreover, with more water produced, flooding is getting heavier. As a result, a greater current density gradient is observed. In general, some factors are co-impacting current density distribution: gas concentration gradient along the channel, GDL flooding extent, membrane impedance, etc., among which the later one is counteractive with the former two. With the influences, the fuel cell shows relative uniform current density distribution at 0.7 V.

3.2. Cell performance in starvation operation

3.2.1. Steady-state behavior

For starvation operation mode of anode and cathode, insufficient flux of hydrogen and air are supplied to the fuel cell, respectively. For anode starvation, flux of H_2 is fixed to be $0.076\,SL\,min^{-1}$, which is only enough for 10 A discharging; flux of air is fixed to be $0.38\,SL\,min^{-1}$, twice the amount needed for 10 A operation. For cathode starvation operation, the situation is on the other way round, flux of H_2 $0.152\,SL\,min^{-1}$ and flux of air $0.19\,SL\,min^{-1}$.

Fig. 4 shows the polarization curves of the fuel cell under anode starvation (a) and cathode starvation (b). In the case of 0.2 MPa (absolute pressure) operation, it was very obvious that the gauge pressure was dropping from 0.1 MPa to 0 MPa during the measurement. For 0.1 MPa operation, we sank the hydrogen tail pipe into a beaker filled with water, during the measurement of polarization curve, in the beginning, the bubbling speeded down, and then water was observed inhaled from the beaker into the transparent plastic gas pipe. This indicated that there was some extent of "vacuum effect" during the starvation, as reported by Kim et al. [8,9]. While for cathode starvation, no vacuum effect was observed. There was almost no pressure dropping for 0.2 MPa operation and gas was always bubbling from the vent pipe for 0.1 MPa operation.

For anode starvation and cathode starvation, this experiment gave quite different polarization curves. As shown in Fig. 4a, the fuel cell shows a unique behavior under anode starvation. As mention above, flux of hydrogen is only enough for 10 A operation, corresponding to $0.33\,A\,cm^{-2}$ current density. However, it is very interesting that, current density in the polarization curve increases to about $0.45\,A\,cm^{-2}$ and then decreases to be $0.35\,A\,cm^{-2}$, forming a "hump" in polarization curve. For cathode starvation, there is no such "hump" in the polarization curves. The curves are just similar to those in regular conditions; difference only lies in that the limiting current density occurs in higher cell voltage region: in regular conditions, limiting current density occurs when cell voltage is lower than 0.5 V, while in cathode starvation, it occurs at about 0.6 V.

This behavior could be explained as the following: although the hydrogen flux is only for 10 A operation, excess

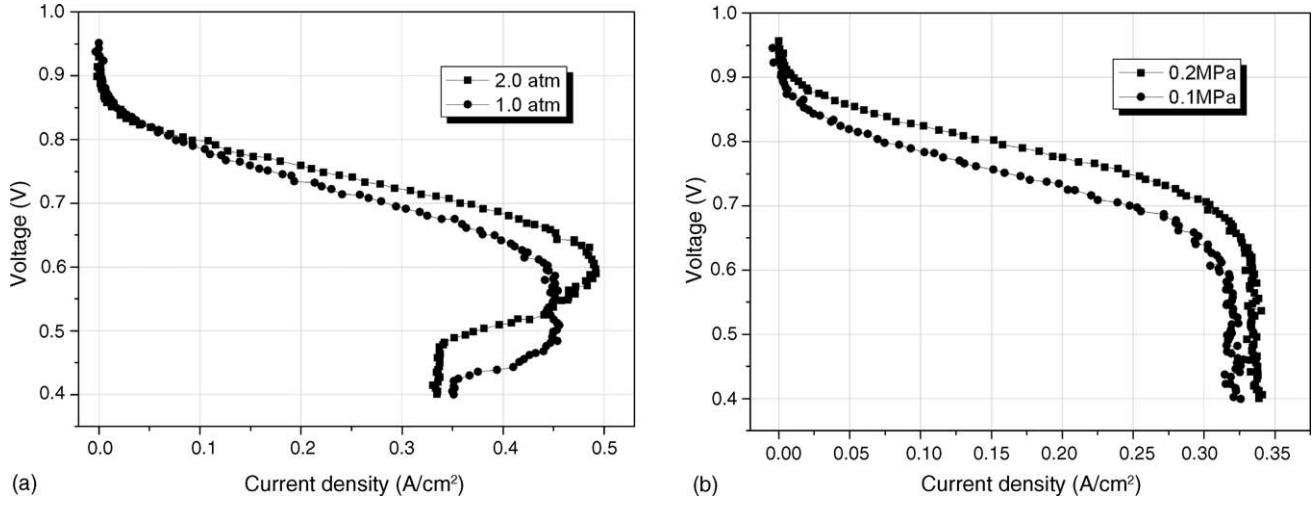

Fig. 4. Polarization curves of fuel cell under 0.1 MPa and 0.2 MPa: (a) anode starvation, flux of H_2: $0.076\,L\,min^{-1}$, flux of air: $0.38\,L\,min^{-1}$ and (b) cathode starvation, flux of H_2: $0.152\,L\,min^{-1}$, flux of air: $0.19\,L\,min^{-1}$.

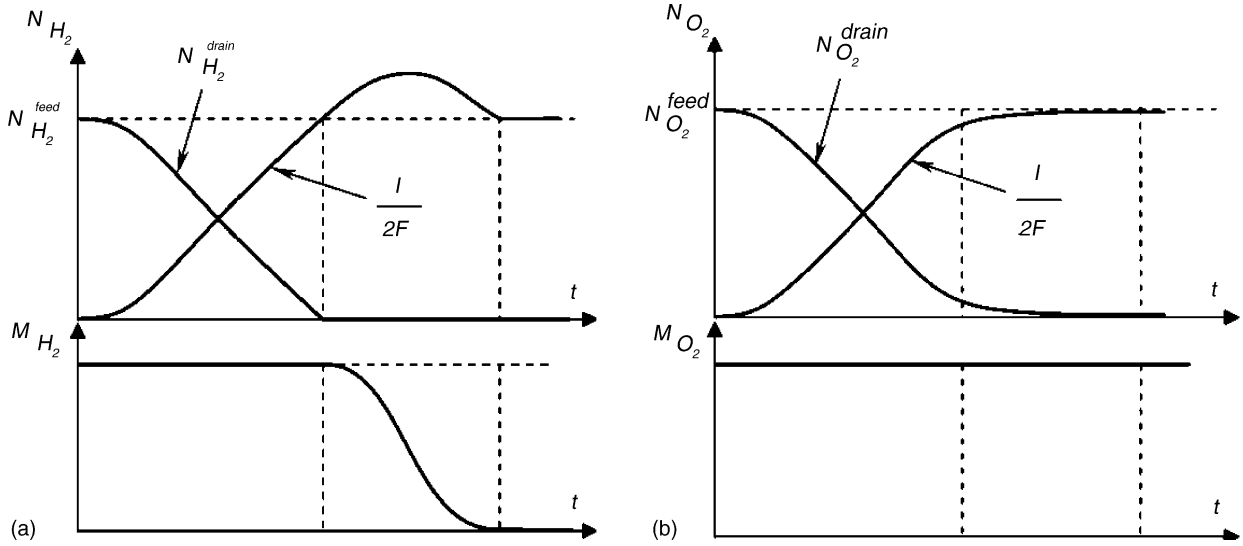

Fig. 5. Illustrations for: (a) anode starvation and (b) cathode starvation.

hydrogen exists in the pipes and flow channels, which act as a hydrogen "reservoir". Because the polarization curve measurement is a linear voltage scan process, which is a quasi-steady process, hydrogen in the "reservoir" will take part in the reaction and contribute to the total current value and so has impact in the shape of polarization curve. The conservation of H_2 in the fuel cell could be expressed:

$$\frac{dM_{H_2}}{dt} = N_{H_2}^{feed} - N_{H_2}^{drain} - \frac{I}{2F} \tag{3}$$

where M_{H_2} is the molar amount of H_2 in the "reservoir", $N_{H_2}^{feed}$ and $N_{H_2}^{drain}$ the stand for molar flux of H_2 fed in and drained out of the fuel cell, respectively, and I is the current value of the fuel cell. Eq. (3) could be rewritten as

$$I = 2F\left(N_{H_2}^{feed} - N_{H_2}^{drain} - \frac{dM_{H_2}}{dt}\right) \tag{4}$$

For cathode starvation, Eq. (4) changes to be:

$$I = 4F\left(N_{O_2}^{feed} - N_{O_2}^{drain} - \frac{dM_{O_2}}{dt}\right) \tag{5}$$

In anode starvation, when cell voltage is relative high, the fed gas is enough for the reaction, and the H_2 in the "reservoir" will not take part in the reaction because of pressure balance. So the last term in Eq. (4) is zero, and the part of H_2 does not oxidized in the electrode will be drained out of the fuel cell. $N_{H_2}^{drain}$ decreases with the increasing of I. When I reaches 10 A, $N_{H_2}^{drain}$ decreases to zero. With the voltage decreasing further, there's vacuum effect because of starvation, pressure in the fuel cell decreases and the extra H_2 in the "reservoir" will take part in the anode reaction. At this time, $N_{H_2}^{drain} = 0$, and $\frac{dM_{H_2}}{dt} < 0$, so current will increase further and be greater than 10 A. With the decreasing of cell voltage and, $\frac{dM_{H_2}}{dt}$ decreases to a minimum value and increases to zero when M_{H_2} is consumed up, so a "hump" is formed. With almost all the H_2 in the "reservoir" consumed, the current will decreased to be 10 A. This process is illustrated in Fig. 5a.

For cathode starvation, the process is a little bit different. Because oxygen takes only one-fifth in air, even in cathode starvation, there will not be vacuum effect. The extra oxygen will not take part in the electrode reaction because the pressure is in balance. So the last term in Eq. (5) is almost equal to zero. Furthermore, O_2 diffuses through GDL to the cathode catalyst layer with the drive of partial pressure difference between the channel and the catalyst surface; when O_2 partial pressure in the channel decreases to too small, the diffusion flux will be too small according to Darcy's Law:

$$N_{O_2} = D_{O_2}\frac{p_{O_2}^{channel} - p_{O_2}^{CL}}{\delta_{GDL}} \tag{6}$$

where N_{O_2} is the oxygen diffusion flux, D_{O_2} the diffusion coefficient, $p_{O_2}^{channel}$ and $p_{O_2}^{CL}$ the oxygen partial pressure in flow channel and on the surface of catalyst layer, respectively, and δ_{GDL} is the thickness of GDL. So the middle term on the right side of Eq. (5) will decrease to very small but not equal to zero even when cell voltage decreases to a very low value. As a result, the cell current will be very close to the limiting current but will not exceed it to form a "hump" as the anode starvation does. This process is shown in Fig. 5b.

To verify the discussion above, a reduced scan rate is employed to measure the polarization curve. It is known that the "hump" in the polarization curve of anode starvation is because of the transient item in Eq. (4) as discussed; when a smaller scan rate is employed, it will take a longer time to consume all the hydrogen in the "reservoir". At the pick point, $\left|\frac{dM_{H_2}}{dt}\right|$ is smaller, so the highest current density at lower scan rate is smaller. In Fig. 6a, it shows that the convexity in the polarization curve gets smaller when scan rate decreases from 1 mV s^{-1} to 0.5 mV s^{-1}. For cathode starvation, the change in scan rate almost has no impact on the polarization curve.

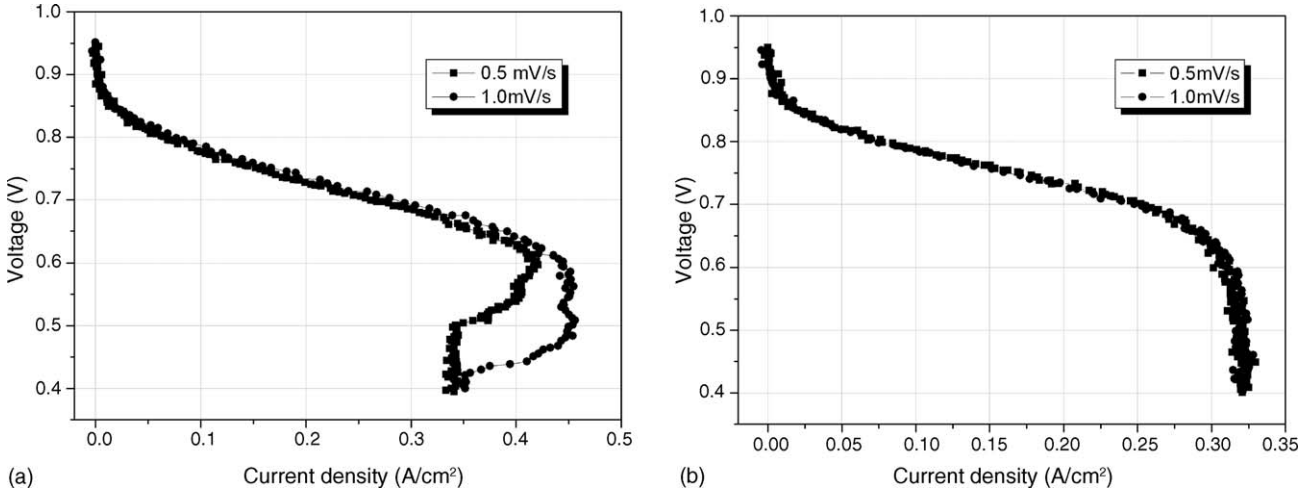

Fig. 6. Polarization curves of the fuel cell with different scan rate under: (a) anode starvation and (b) cathode starvation.

With the discussion above, it will be interesting to think about the current density distribution in starvation. Take anode starvation, for example, there are two possibilities: on one hand, the vacuum effect might level the pressure difference along the flow channel and results in relatively uniform current density distribution; on the other hand, the hydrogen might be consumed so fast that there's no fuel available at the outlet region, which will lead the current density at the outlet region to be zero. Experiments will prove which possibility is true.

The polarization curves of the subcells are recorded simultaneously with the overall cell polarization curve given in the former section. Fig. 7 shows the curves of the subcells in the middle column in starvation operation. Plot (a) illustrates that, in anode starvation, current density of fourth row of subcells (the nearest row to the outlet, in Fig. 7 only show subcell 11 for representation) drops to zero first, and then with the voltage getting lower, current of the third row drops to zero. It seems there's little impact on the first and second row. This behavior confirms the second possibility given above, that is to say, in anode starvation, current density of the starved region will decrease to zero and the non-starved region will have little impact. It could also be seen in Fig. 7a that, the current density drops suddenly to zero, the polarization curves are almost the same to those in Fig. 2 before dropping. The reason lies in that the anode gas is pure hydrogen, without dilution effect of other inert gas like nitrogen in air.

For cathode starvation, not same to the occasion of anode starvation, Fig. 7b shows that the starvation has impact on all the subcells. From relatively high voltage, 0.8 V, the fourth row shows suffering from the oxygen concentration drop. And then the third row at about 0.72 V. When the cell voltage is getting lower, current density of the fourth and third row is becoming smaller, forming a little convexity in the polarization curve, analogous to that in Figs. 4a and 6a. It is easy to understand that, when air is not enough, oxygen concentration dropping fast, everywhere inside the fuel cell will surfer from the concentration decreasing. With the decreasing

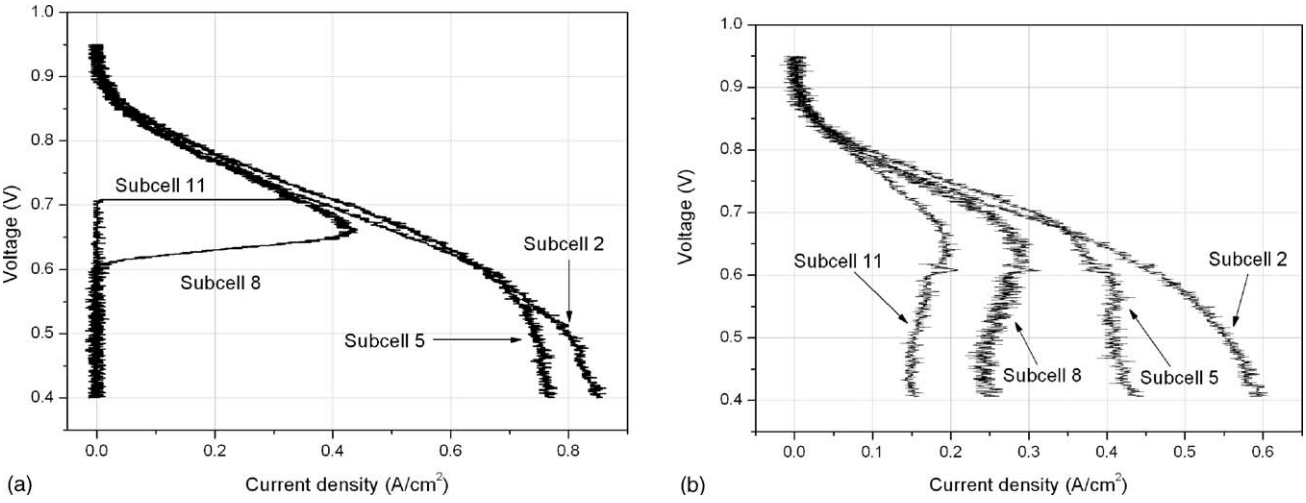

Fig. 7. Polarization curves of the subcells in the middle column under: (a) anode starvation and (b) cathode starvation.

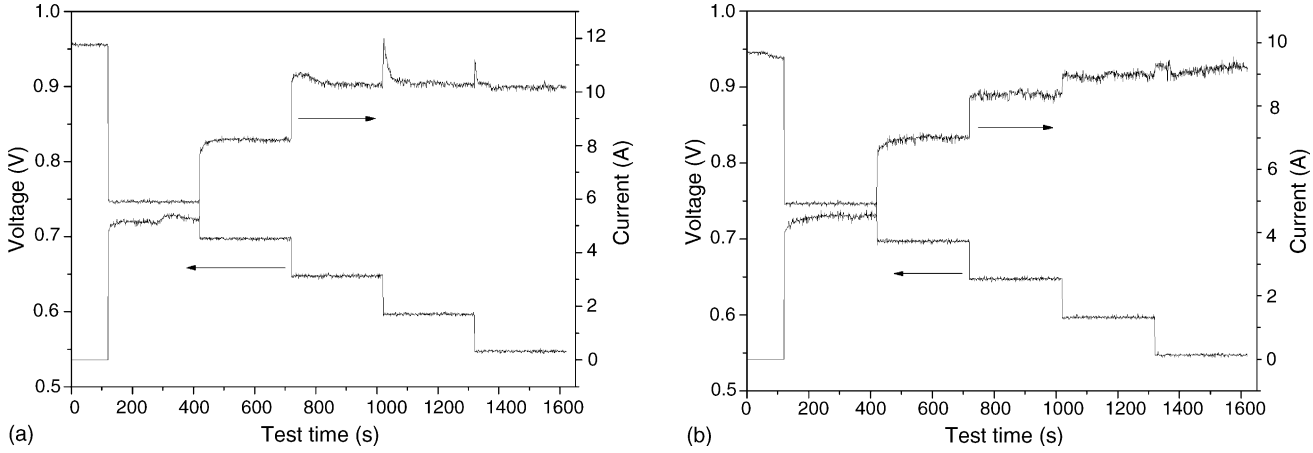

Fig. 8. Dynamic behavior of the fuel cell under: (a) anode starvation (b) cathode starvation.

of cell voltage, current in the inlet region increases with the least impact of oxygen concentration dropping, which will make oxygen thinner in the outlet region, so current density decreases and convexity forms in the polarization curve. Even this, no zero current density regions were observed. But it is not sound to say that there will not be zero current regions in cathode starvation. In some cases, like poor flow channel design or flow channel block with flooding, current density might be zero in those regions where air cannot flow to.

3.2.2. Transient behavior

Transient behavior of the overall cell and the subcells was tested with constant voltage step discharging. Voltage of the cell varies from 0.75 V to 0.55 V with five steps, each step lasted 5 min. Fig. 8 demonstrates the transient behavior of the overall cell voltage and current. Fig. 9 shows the transient current behavior of the subcells. In Fig. 8a, which is the occasion for anode starvation operation, it is shown that when cell voltage drops from the open circuit voltage to 0.75 V and from 0.75 V to 0.7 V, the current jumps up to certain value, then increases slowly to form an arc. It is easy to understand that, when cell voltage drops suddenly, H_2 on the catalyst surface is consumed very fast, to form a H_2 concentration gradient across the GDL. After hydrogen diffusion corresponds to the change to reduce the gradient, current increase gradually. However, the transient behavior of the voltage drop from 0.7 V to 0.65 V is a little bit different. The current increases to a little bit higher than 10 A and then drops gradually to 10 A to form a small convexity, which is similar to those in Figs. 4a and 6a and have been discussed in the former section. The difference is those two plots are linear voltage scan and here is constant voltage operation. For the case of 0.65–0.6 V and 0.6–0.55 V, the voltage drop causes the current increases suddenly, while there is no enough reactant for the reaction, current drops gradually to form a little pinnacle.

For cathode starvation, there is large current jump when cell voltage decreases from 0.75 V to 0.7 V and from 0.7 V to 0.65 V, same as the anode starvation case. But from 0.65 V to 0.6 V, current increases less than 1 A. Even when cell voltage drops to 0.55 V, the current is about only 9 A. Oxygen in the cathode gas is not fully consumed as hydrogen in anode, at 0.55 V, there is about 2% O_2 left and drained out of the fuel

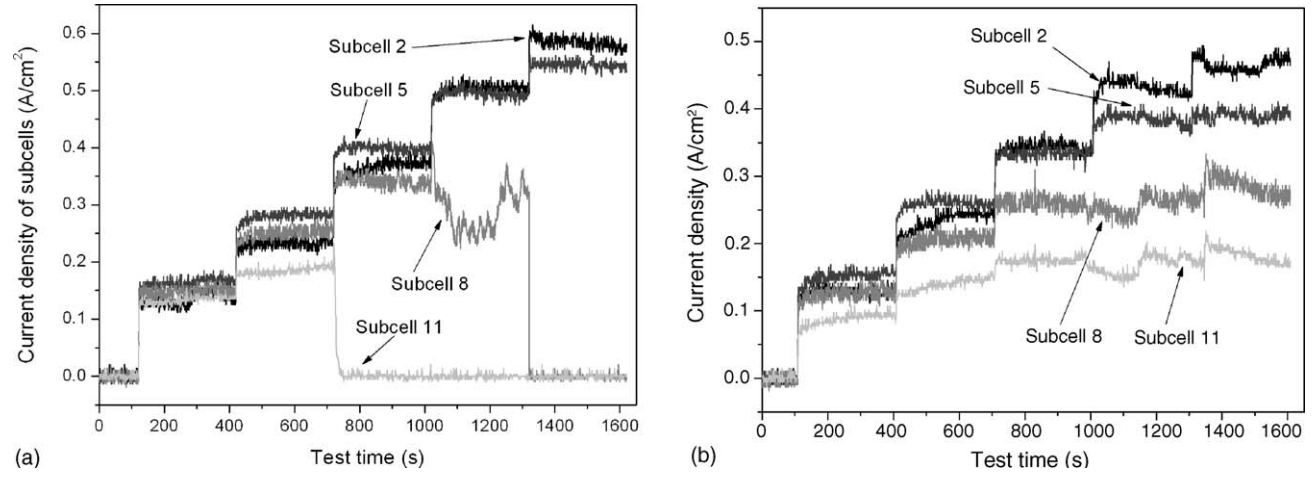

Fig. 9. Dynamic behavior of the subcells in the middle column under: (a) anode starvation and (b) cathode starvation.

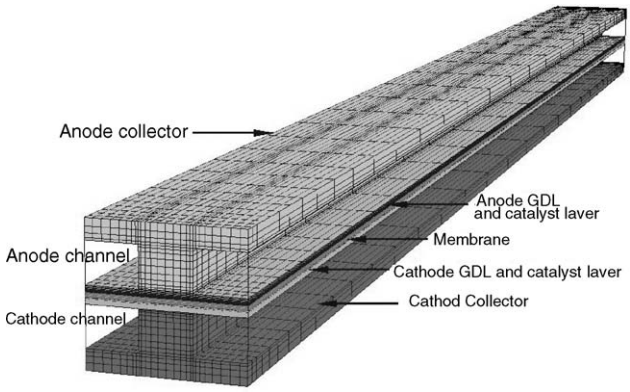

Fig. 10. Simulation region and calculation grid.

cell. Because of the dilution effect of nitrogen in air, it is not likely that all the oxygen in the cathode gas is consumed and no oxygen in the vent gas.

The transient performance of the subcells is shown in Fig. 9. In anode starvation case, when cell voltage decreases from 0.7 V to 0.65 V, current density of the subcell 11 drops to zero, indicate that hydrogen is consumed up in the upper three rows of subcells. When voltage drops from 0.65 V to 0.6 V, current density of subcell 8 jumps from about 0.33 A cm^{-2} to 0.4 A cm^{-2}, but the extra hydrogen in this position is consumed up very soon, so current could not maintain and then drops. As a result, a current pinnacle is formed as shown in Fig. 8a. Transient behavior of the subcells in cathode starvation is depicted in Fig. 9b. It shows that when voltage steps down, current density of the outlet region does not show obvious jumping behavior. When voltage gets lower, higher electrode overpotential will accelerate the electrochemical reaction and current will increase obviously. However, in cathode starvation, oxygen concentration on the catalyst layer is very low even it is not zero. Oxygen diffusion is the limiting step. So lower cell voltage does not influence current density too much. In real fuel cell operation, a relative high stoichiometric ratio is often adopted to minimize the influence mass transfer, even with the expense of increasing power for air fan or compressor.

4. Starvation operation simulation

4.1. Simulation method

Simulation of the fuel cell in starvation operation was conducted with commercial CFD software CFD-ACE+ V2003. This software has been used by some research groups and companies including Ballard Power System for fuel cell modeling [20,21]. The model equations could be found in other documents [21,22]. Here, we use it to simulate the starvation process of fuel cell.

The simulation region and the grid are shown in Fig. 10. The dimension of the simulation region is 3 mm (width) × 50 mm (length) × 2.94 mm (height), which is a slice of the fuel cell including a MEA (two GDLs, two catalyst layers and a membrane), two half-H2-channels and two half-air-channels, and two T-shape collectors. The calculation grids of the solid domains are also shown in the plot. Note that the grid of the channel is not shown in the figure.

In this simulation, some basic assumptions are used: the gas mixture is ideal and flow type is laminar; water exists

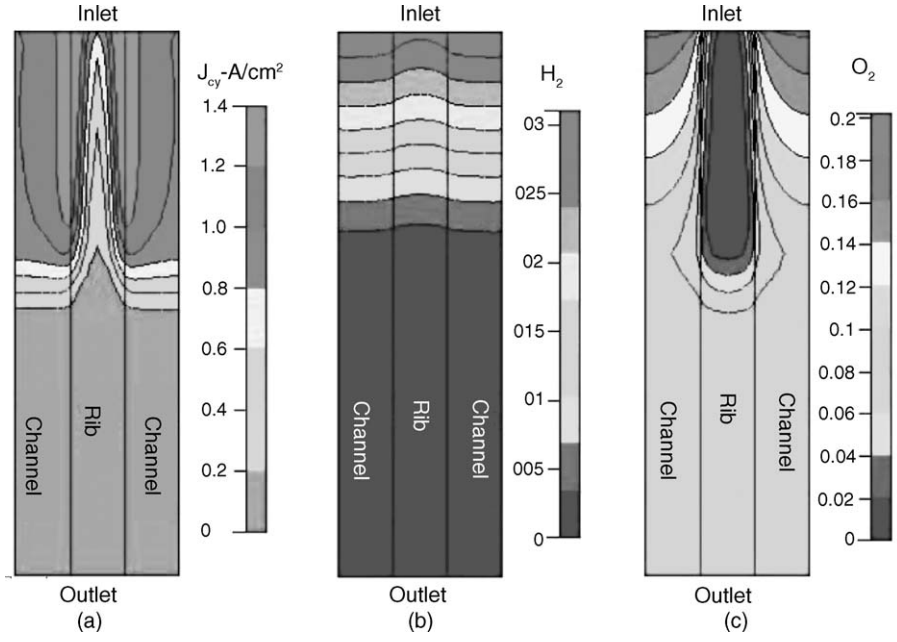

Fig. 11. Contour plots for anode starvation simulation results: (a) current density distribution in membrane, (b) mass fraction of H_2 on the surface of anode catalyst layer and (c) mass fraction of O_2 on the surface of cathode catalyst layer. Cell temperature: 343 K; outlet pressure: 0.2 MPa; hydrogen and air humidity: 90%; anode inlet velocity: 0.036 m s^{-1}; cathode inlet velocity: 0.182 m s^{-1}; cell overpotential: −0.6 V.

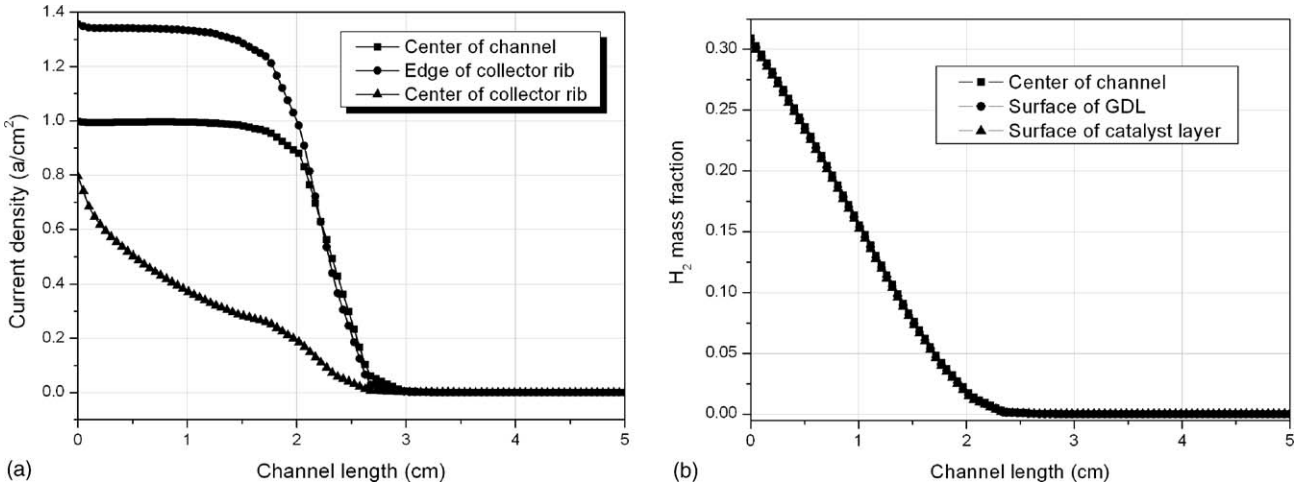

Fig. 12. Current density (a) and H_2 mass fraction (b) along the lines at different positions for anode starvation. Operation conditions are same to Fig. 11.

only in vapor phase; membrane is impermeable for gases; the effects of gravity are ignored.

Boundary conditions: profiles of the channel center are symmetry boundary; the top face is the surface of anode collector, isothermal wall condition is set with 343 K and 0 V potential; the bottom cathode collector surface is also isothermal wall with 343 K, the overpotential is −0.6 V; the front and back face are also isothermal wall; the other faces inside are interfaces. Volume conditions for collectors are solid, for channels GDLs, catalyst layers and membrane are fluid; the five layers in the MEA is porous media, parameters are listed in Table 1.

For anode starvation operation, velocity of the anode inlet is 0.036 m s^{-1} and cathode inlet 0.182 m s^{-1}; for cathode starvation, H2 velocity 0.072 m s^{-1}, air velocity 0.091 m s^{-1}.

4.2. Simulation results

Fig. 11 shows the simulation results for anode starvation operation. Note that in this figure and the following Fig. 13, the plots are drawn from the top view. For clarity, the length of the channel direction is scaled down to 1/5. Plot (a) shows the membrane phase current density distribution in the horizontal profile of the membrane. It is very clear that the current is concentrated in the first half of the fuel cell from the inlet, and current of the outlet half is almost zero. The region with the highest current density is at the rib edge. Current density

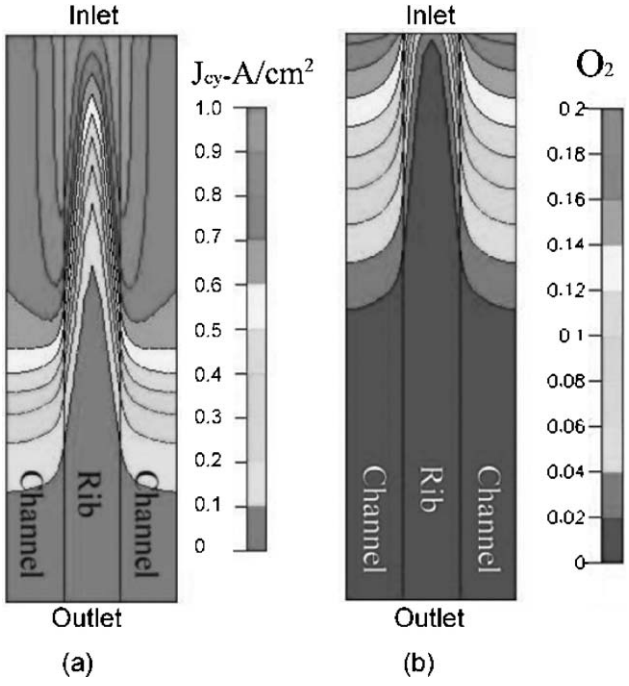

Fig. 13. Contour plots for cathode starvation simulation results: (a) current density distribution in membrane and (b) mass fraction of O_2 on the surface of cathode catalyst layer. Cell temperature: 343 K; outlet pressure: 0.2 MPa; hydrogen and air humidity: 90%; anode inlet velocity: 0.072 m s^{-1}; cathode inlet velocity: 0.091 m s^{-1}; cell overpotential: −0.6 V.

Table 1
Model parameters

Parameter	Value	Parameter	Value
Channel length (m)	5.0×10^{-2}	Porosity of catalyst layer	0.6
Height of gas channel (m)	8.0×10^{-3}	Porosity of membrane	0.2
Channel width (m)	2.0×10^{-3}	Permeability of GDL and catalyst layer (m^2)	1.0×10^{-11}
Collector rib width (m)	1.0×10^{-3}	Permeability of membrane (m^2)	1.0×10^{-18}
Thickness of GDL (m)	2.0×10^{-4}	Temperature of fuel cell (K)	343
Thickness of catalyst (m)	2.0×10^{-5}	Pressure of anode and cathode gas (MPa)	0.1
Thickness of membrane (m)	1.0×10^{-4}	Temperature of feed gas (K)	343
Porosity of GDL	0.7	Relative humidity of feed gas (%)	90

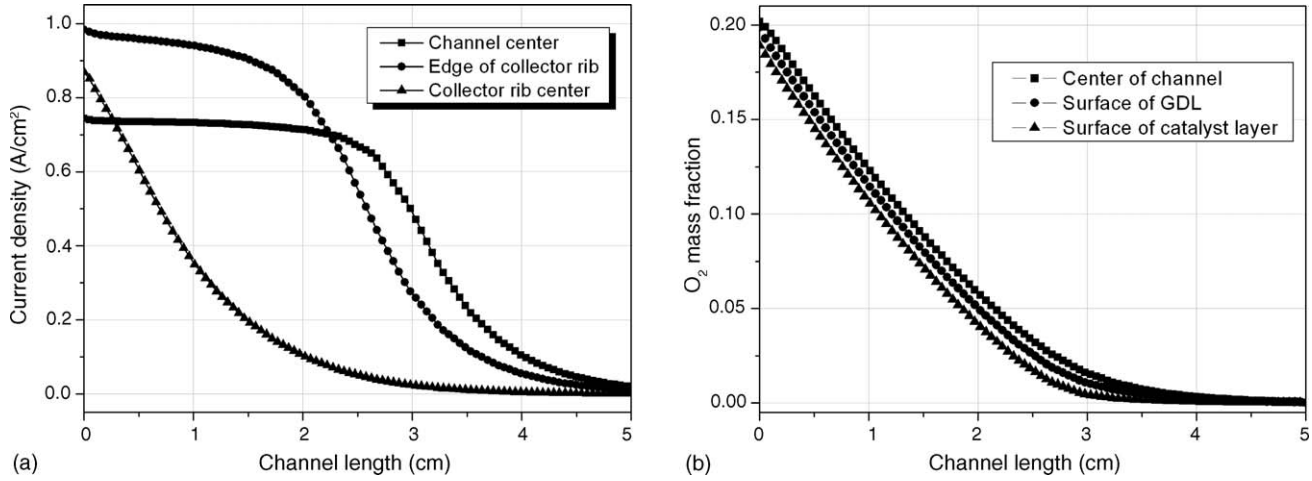

Fig. 14. Current density (a) and H_2 mass fraction (b) along the lines at different positions for cathode starvation. Operation conditions are same to Fig. 13.

under the rib is much lower than that under the channel at the same position from the inlet, forms a shape like fire. The current density distributions along three lines parallel to the channel are also shown in Fig. 12a, in which we can see that from the inlet ($L = 0$ cm) to $L = 2$ cm, the current density at the collector rib edge is much higher than that under the channel and under the rib. From $L = 2$ cm to 3 cm, current density decreases rapidly, and from $L = 3$ cm to 5 cm, current density along the three lines are all equal to zero. The current density distribution trend is just the same to the experimental results for anode starvation. The non-starved region has excellent cell performance, while current density of the starved region is zero. Fig. 11b shows the hydrogen mass fraction on the surface of the anode catalyst layer, for most regions to the outlet side, hydrogen mass fraction is zero. Fig. 12b shows hydrogen mass fraction along three lines parallel to the channel: center of channel, surface of GDL and surface of catalyst layer. It shows that the three lines almost overlap each other, which indicates very small hydrogen concentration difference at the same length at the three positions. When $L = 2$ cm, hydrogen becomes very thin and the current density begins to drop sharply. When $L = 3$ cm, hydrogen concentration is almost zero, no hydrogen is available for the electrode reaction, so current is zero. Fig. 11c depicts oxygen mass fraction on the surface of cathode catalyst layer. It shows that for the non-starved region, there is great oxygen concentration gradient along the channel and vertical to the channel. Under the rib of the inlet region, oxygen concentration is almost zero because of oxygen consumption and slow oxygen diffusing through the GDL. This is the reason for the formation of the fire-shaped current density distribution under the rib of the inlet region. For the non-starved region, oxygen concentration is constant because no oxygen consumed for lack of hydrogen in anode.

Figs. 13a and 14a show the current density distribution of the cell in cathode starvation. The highest current density is less than 1.0 A cm^{-2}, much lower than 1.35 A cm^{-2} in the anode starvation case. From $L = 2$ cm, current is decreasing gradually, not as shapely as Fig. 12a. When $L > 4$ cm, current density is very low, but no zero current density region is found. Figs. 13b and 14b show the oxygen mass fraction distribution. For most regions near the outlet and under the rib, oxygen concentration is very low, but not zero. It also shows oxygen gradient from the center of the channel to the catalyst layer surface. Because of the diffusion of oxygen, there's no zero current density region for cathode starvation, which is same to the experimental results.

5. Conclusions

For fuel cell operation, starvation will have important influence to the cell performance and might bring safety issue. Fuel and oxidant starvation behavior of a 30 cm^2 PEMFC is studied with current density distribution measurement approach. Experiments prove that the fuel cell will perform different behavior in anode and cathode starvation. In anode starvation, the fuel cell exhibits unique polarization curve, with a "hump" in the curve where current exceeds the given flux stoichiometry, which is not found in the polarization curve of cathode starvation. Vacuum effect is confirmed in anode starvation and proper explanation has been given. The fuel cell also exhibits different current density distribution behavior in starvation. In anode starvation, current density of the starved region decrease to zero, with the non-starved region little impacted. While the cathode starvation makes all the fuel cell influenced, and no zero current regions observed. Numerical simulation results with CFD-ACE+ give the same behavior of the fuel cell in starvation.

Acknowledgement

Finical support by "National 973 Project on Hydrogen Energy (TG2000026410)" and "Open Funding of the State Key Laboratory of Automotive Safety and Energy" are gratefully acknowledged.

References

[1] S.D. Knights, K.M. Colbow, J.S. Pierre, D.P. Wilkinson, J. Power Sources 127 (2004) 127–134.
[2] K. Mitsudo, T. Murahashi, J. Electrochem. Soc. 137 (1990) 3079–3085.
[3] K. Mitsudo, T. Murahashi, J. Appl. Electrochem. 21 (1991) 524–530.
[4] A. Lundblad, P. Bjornbom, J. Electrochem. Soc. 139 (1992) 1337–1342.
[5] R.H. Song, C.S. Kim, D.R. Shin, J. Power Sources 86 (2000) 289–293.
[6] M. Fowler, R.F. Mann, J.C. Amphlett, B.A. Peppley, P.R. Roberge, in: W. Vielstich, H.A. Gasteiger, A. Lamm (Eds.), Handbook of Fuel Cells—Fundamentals, Technology and Applications, vol. 3, John Wiley & Sons, Ltd., 2003, p. 663.
[7] A. Taniguchi, T. Akita, K. Yasuda, Y. Miyazaki, J. Power Sources 130 (2004) 42–49.
[8] S. Kim, S. Shimpalee, J.W. van Zee, J. Power Sources 135 (2004) 110–121.
[9] S. Kim, S. Shimpalee, J.W. van Zee, J. Power Sources 137 (2004) 43–52.
[10] Z.X. Liu, Z.Q. Mao, B. Wu, L.S. Wang, V.M. Schmidt, J. Power Sources 141 (2005) 205–210.
[11] J. Stumper, S.A. Campbell, D.P. Wilkinson, M.C. Johnson, M. Davis, Electrochim. Acta 43 (1998) 3773–3783.
[12] Ch. Wieser, A. Helmbold, E. Gülzow, J. Appl. Electrochem. 30 (2000) 803–807.
[13] M. Noponen, T. Mennola, M. Mikkola, T. Hottinen, P. Lund, J. Power Sources 106 (2002) 304–312.
[14] M.M. Mench, C.Y. Wang, J. Electrochem. Soc. 150 (2003) A79–A85.
[15] M.M. Mench, C.Y. Wang, M. Ishikawa, J. Electrochem. Soc. 150 (2003) A1052–A1059.
[16] A. Hakenjos, H. Muenter, U. Wittstadt, C. Hebling, J. Power Sources 131 (2004) 213–216.
[17] Y.G. Yoon, W.Y. Lee, T.H. Yang, G.G. Park, C.S. Kim, J. Power Sources 118 (2003) 193–199.
[18] S.S. Kocha, in: W. Vielstich, H.A. Gasteiger, A. Lamm (Eds.), Handbook of Fuel Cells—Fundamentals, Technology and Applications, vol. 3, John Wiley & Sons, Ltd., 2003, p. 538.
[19] B. Wu, K.Y. Ge, X.Y. Zheng, L.S. Wang, Z.X. Liu, Proceedings of the 8th Asian Hydrogen Energy Conference, Beijing, 2005, p. 218.
[20] S.W. Cha, R. O'Hayre, Y. Saito, F.B. Prinz, J. Power Sources 134 (2004) 57–71.
[21] A. Su, Y.C. Chiu, F.B. Weng, Int. J. Energy Res. 29 (2005) 409–425.
[22] CFD-ACE+ Version 2003 User Manual, CFD Research Corp., Huntsville, AL 35805.